Geophysical and Production Data History Matching Based on Ensemble Smoother with Multiple Data Assimilation

Zelong Wang[1, 2, 3, *], Xiangui Liu[1, 2, 3], Haifa Tang[3], Zhikai Lv[3] and Qunming Liu[3]

Abstract: The Ensemble Kalman Filter (EnKF), as the most popular sequential data assimilation algorithm for history matching, has the intrinsic problem of high computational cost and the potential inconsistency of state variables updated at each loop of data assimilation and its corresponding reservoir simulated result. This problem forbids the reservoir engineers to make the best use of the 4D seismic data, which provides valuable information about the fluid change inside the reservoir. Moreover, only matching the production data in the past is not enough to accurately forecast the future, and the development plan based on the false forecast is very likely to be suboptimal. To solve this problem, we developed a workflow for geophysical and production data history matching by modifying ensemble smoother with multiple data assimilation (ESMDA). In this work, we derived the mathematical expressions of ESMDA and discussed its scope of applications. The geophysical data we used is P-wave impedance, which is typically included in a basic seismic interpretation, and it directly reflects the saturation change in the reservoir. Full resolution of the seismic data is not necessary, we subsampled the P-wave impedance data to further reduce the computational cost. With our case studies on a benchmark synthetic reservoir model, we also showed the supremacy of matching both geophysical and production data, than the traditional reservoir history matching merely on the production data: the overall percentage error of the observed data is halved, and the variances of the updated forecasts are reduced by two orders of the magnitude.

Keywords: History matching, data assimilation, inverse modeling, ESMDA.

1 Introduction

As many of the oil fields come to the late stage of production, in order to achieve a higher recovery of the hydrocarbon, secondary or tertiary production is introduced, by injecting water or gas, or even chemicals to the reservoir. For heavy oil, hot steam injection or formation combustion may also be conducted. Due to the complexity and the heterogeneity of the reservoir, the improved oil recovery operation methods may still leave the bypass hydrocarbon zone upswept, resulting a low recovery factor.

In order to have a successful operation for those brown fields, more detailed and accurate

[1] University of the Chinese Academy of Sciences, Beijing, 100049, China.

[2] Institute of Porous Flow and Fluid Mechanics, The Chinese Academy of Sciences, Langfang, 065007, China.

[3] Petro China Research Institute of Petroleum Exploration and Development, Beijing, 100083, China.

[*] Corresponding Author: Zelong Wang. Email: wangzel69@petrochina.com.cn.

Received: 31 October 2019; Accepted: 04 December 2019.

reservoir characterizations are essential. Inverse reservoir modeling, is also known as history matching, with abundant production data will significantly increase the certainty of the reservoir models. Recently, researchers have developed different numerical methods for the reservoir simulation, such as Wang et al. [Wang and Sun (2016); Wang, Sun and Yu (2017); Wang, Sun, Gong et al. (2018); Wang (2019); Wang, Wang and Chen (2019)], made the numerical simulation very reliable, so the challenges are more on the geological modeling. Traditionally, geologists may build one deterministic static reservoir model, and reservoir engineers manually change the geological and PVT parameters to match the production data, this would result in an unrealistic representation of the "true" reservoir, even though the production history was matched, the forecasts from the model would be unreliable. Thanks to the high speed computing technology, recent reservoir modeling has been evolved into probabilistic modeling or statistical modeling. People generated a set of initial reservoir models (e.g., 100 models), each model is called a realization of the reservoir. The ensemble of those realizations represents the possible outcomes of the real petroleum reservoir.

Computer assisted history matching can update those initial reservoir models, by honoring the history production data, thus the updated reservoir models would have a higher certainty of the true reservoir parameters, and the forecasts therefore will be more reliable. In recent decades, ensemble-based history matching methods have become very popular, such as the ensemble Kalman filter (EnKF) [Nævdal, Johnsen, Aanonsen et al. (2005); Aanonsen, Nævdal, Oliver et al. (2009)], ensemble smoother (ES) [Van Leeuwen and Evensen (1996)], the ensemble Kalman smoother (EnKS) [Evensen and van Leeuwen (2000)] and their iterative versions [Gu and Oliver (2007); Li and Reynolds (2009); Emerick and Reynolds (2012a); Chen and Oliver (2013); Luo, Stodral, Lorentzen et al. (2015)]. Those methods share the advantages of simplicity, flexibility in implementation, and easier uncertainty quantification over the gradient methods [Bhakta, Luo and Nævdal (2016)].

It is also important to acquire the detailed knowledge of the reservoir saturation profile, the fluid distribution and the fluid pass ways. Static, or one-time measurements of the reservoir properties cannot meet the need of recent reservoir management workflows, reservoir engineers seek to time-depend information from a variety of oilfield disciplines which assist to constrain, and to improve the accuracy of reservoir models and fluid distribution. Time-lapse saturation logging and permanent downhole gauges can continuously monitor some reservoir properties at the well locations, and the 4D seismic (also called as time lapsed seismic), which can observe the change of fluid at the field scale. 4D seismic is the seismic surveys acquired at the same field at different times over the production time of a reservoir, to present the snapshots of the fluid saturation and distribution. Before 4D seismic, a base-line 3D seismic survey on the reservoir before production should be conducted, rock physics models are established, and 4D feasibility studies on synthetic seismic amplitude responses to variations in reservoir conditions to decide which 4D signal that rock and fluid will be generated. There are some case studies about 4D seismic survey to optimize waterflooding in oilfield such as Ekofisk et al. [Talukdar and Instefjord (2008); Helland, Festervoll, Stronen et al. (2008); Lumley, Adams, Meadows et al. (2008); Tolstukhin, Lyngnes and Sudan (2012)].

Conventionally, it is quite challenging to integrate 4D geophysical data in to the workflow of ensemble based history matching methods, due to the inconsistency of the intrinsic data properties of the production data and 4D seismic data: production data is scarce spatial and dense in time, yet the 4D seismic data is dense in spatial and scarce in time. For example, with EnKF, as proved in Reynolds' et al. [Reynolds, Zafari and Li (2006)] and Emerick's et al. [Emerick and Reynolds (2012a)] work, by assimilating time-dense production data, the process works at each time step, one Gauss-Newton (GN) solution is obtained to each reservoir realizations in the ensemble states, and because the production data is sufficient in data, EnKF can accumulate several GN corrections, gradually updated the reservoir models with the constraint of the production data; however, the time-scarce seismic data would not have the same sufficient data assimilation time steps.

In this paper, we integrated 4D seismic data into the production history matching, by applying a new algorithm come up with by Emerick et al. [Emerick and Reynolds (2012b)], ensemble smoother with multiple data assimilation (ESMDA) on a synthetic sandstone reservoir with waterflooding operation. Instead of sequentially assimilate the data as in EnKF, ESMDA assimilate all the data set in one run, including both the production data and time-lapse geophysical data, thus avoid the inconsistency of the step assimilation of production and geophysical data. By arbitrarily set the times of data assimilation, Emerick et al. [Emerick and Reynolds (2012b)] proved the multiple data assimilation is similar to an iterative ES with smaller GN corrections.

2 Methodology

We first formulate the EnKF and ES formulas, from there we derived the set of equations of ESMDA. We then discuss its scope of applications, and lastly we compared it with EnKF, showing its potential application in geophysical and production data history matching.

2.1 Ensemble kalman filter (EnKF)

The EnKF is a Monte Carlo method based on Markov chain approach. First, it samples many realizations from the prior probability density function (PDF). Second, for each realization, it uses the model forecast function (in history matching, the forecast function is the reservoir simulator) to estimate the dynamic data at the next time step. Third, it uses those updated reservoir realizations to calculate the approximation of the predicted covariance.

For the equations in this paper, we denote a vector or a matrix with a bold font, and a scalar with a plaintext. In the application in reservoir history matching, here we define the extended state variable xk as the parameter to be estimated at the time step k, which contains reservoir static geological parameters, dynamic parameters, and measurement data.

$$\boldsymbol{x_k} = \begin{pmatrix} \boldsymbol{m_k} \\ \boldsymbol{P_k} \\ \boldsymbol{d_k} \end{pmatrix} \tag{1}$$

where $\boldsymbol{m_k}$ is the estimation of static geological parameters at the time k, which dimension is $N_m \times 1$; $\boldsymbol{P_k}$ is the dynamic parameters (e.g., reservoir pressure, fluid saturation, etc.), which dimension is $N_p \times 1$; $\boldsymbol{d_k}$ is the measurement data (e.g., oil rate, water rate, bottom-hole pressure, or 4D seismic data), which dimension is $N_n \times 1$. N_m, N_p, N_n are the number of static parameters in a single reservoir realization, the number of dynamic parameters at a single time step, and the number of measurement at that time step respectively.

The EnKF consists of two sets of equations: the state forecast equation, and the update equation. The forecast equations are:

$$\boldsymbol{d_k^f} = \boldsymbol{f}\left(\boldsymbol{\hat{x}_{k-1}}^{\boldsymbol{u}}\right) \tag{2}$$

$$\boldsymbol{\hat{x}_k}^{\boldsymbol{f}} = \boldsymbol{\hat{x}_{k-1}}^{\boldsymbol{u}} \tag{3}$$

where the function f(x) represents the reservoir fluid simulation. Assume the fluid PVT properties and the production schedule stays the same, the forecast is determined by the reservoir dynamic parameters at the previous time step, which means the extended state variable $\boldsymbol{\hat{x}_{k-1}}^{\boldsymbol{u}}$ contains all the information of the input to the reservoir fluid simulator; $\boldsymbol{d_k^f}$ is the forecast from the simulator. The superscript f and u stand for "forecast" and "update" respectively, indicate the variable is at the forecast or update stage of the EnKF method.

The update equations are:

$$\boldsymbol{\hat{x}_k}^{\boldsymbol{u}} = \boldsymbol{\hat{x}_k}^{\boldsymbol{f}} + \boldsymbol{C_k^f H^T}\left(\boldsymbol{H C_k^f H^T} + \boldsymbol{R}\right)^{-\boldsymbol{1}}(\boldsymbol{d_k^f} - \boldsymbol{d_k^o}) \tag{4}$$

where $\boldsymbol{C_k^f}$ is the covariance matrix of $\boldsymbol{\hat{x}_k}^{\boldsymbol{f}}$, with the dimension of $N_n \times (N_n + N_m + N_p)$; R is the measurement error (regarded as white noise) covariance matrix, with the dimension of $N_n \times N_p$; $\boldsymbol{d_k^o}$ is the measurements at time step k, H is the linearization operator, which can be expressed as

$$\boldsymbol{H} = [\boldsymbol{O}\ \boldsymbol{I}] \tag{5}$$

where O is the null matrix, which dimension is $N_n \times (N_n + N_m)$; I is the identity matrix, which dimension is $N_n \times N_p$.

For the simplicity of the expression, people define Kalman gain K matrix as

$$\boldsymbol{K} = \boldsymbol{C_k^f H^T}\left(\boldsymbol{H C_k^f H^T} + \boldsymbol{R}\right)^{-\boldsymbol{1}} \tag{6}$$

Therefore Eq. (4) can be expressed as

$$\boldsymbol{\hat{x}_k}^{\boldsymbol{u}} = \boldsymbol{\hat{x}_k}^{\boldsymbol{f}} + \boldsymbol{C_k^f H^T}\left(\boldsymbol{H C_k^f H^T} + \boldsymbol{R}\right)^{-\boldsymbol{1}}(\boldsymbol{d_k^f} - \boldsymbol{d_k^o}) \tag{7}$$

As the formulation of the EnKF shows, it require a large time series data to be assimilated in order to sufficiently update the prior model. This means highly computational cost on running the reservoir simulation for tremendously many times. Moreover, EnKF has to storage of the intermediate variables, which are required in restarting the reservoir simulator, and potentially may cause the inconsistency of the full-step and step-wise simulations.

2.2 Ensemble smoother (ES)

The ensemble smoother (ES) is an ensemble based method for data assimilation, it can be applied in petroleum reservoir history matching. Similar to ensemble Kalman filter (EnKF), ES uses an ensemble to approximate the mean and the variance, and applies a variance-minimizing update scheme. There are many literatures discussed the EnKF for data assimilation, while the application of the ES is much less.

Van Leeuwen et al. [Van Leeuwen and Evensen (1996)] proposed ES, in comparison with the recursive updating scheme of EnKF by assimilating data in time, ES estimates the global update in space-time domain in one go, to avoid the recursive updating of the realizations by restarting the reservoir simulator. In nonlinear dynamic models, and especially with chaotic dynamics, EnKF works better than ES because the sequential updates on the ensemble keep the model close to the true solution represented by the observations [Skjervheim and Evensen (2011)].

In petroleum reservoir history matching problems, with ES, because the elimination of restarting the simulation, there is no need to store the state variables such as reservoir pressure and fluid saturation, we only need to update geological parameters (e.g., permeability, porosity) $\boldsymbol{m_k}$. The forecast equations are:

$$\boldsymbol{d^f} = \boldsymbol{g}(\boldsymbol{\widehat{m}^u}) \tag{8}$$

$$\boldsymbol{\widehat{m}_k}^{\boldsymbol{f}} = \boldsymbol{\widehat{m}_{k-1}}^{\boldsymbol{u}} \tag{9}$$

where the function $\boldsymbol{g}(\boldsymbol{x})$ represents the reservoir fluid simulation, all time steps forecasts are included in a large vector $\boldsymbol{d^f}$. Pay attention that the $\boldsymbol{d^f}$ is different from $\boldsymbol{d_k^f}$ of the EnKF equations as previously discussed, whereas $\boldsymbol{d_k^f}$ is the measurement data only at the time step *k*. $\boldsymbol{d^f}$ and $\boldsymbol{d_k^f}$ has the following relationship:

$$\boldsymbol{d^f} = [\boldsymbol{d_1^f}, \boldsymbol{d_2^f}, \boldsymbol{d_3^f}, \cdots, \boldsymbol{d_t^f}]^{\boldsymbol{T}} \tag{10}$$

The standard ES updating formula is shown in Eq. (11)

$$\boldsymbol{m_j^a} = \boldsymbol{m_j^f} + \boldsymbol{C_{MD}^f}(\boldsymbol{C_{DD}^f} + \boldsymbol{R})^{-1}(\boldsymbol{d_{uc,j}} - \boldsymbol{d_j^f}) \tag{11}$$

for *j*=1, 2, …, *Ne* with *Ne* denoting the number of the ensemble members, the super script *a* and *f* indicate the updated state and the prior state respectively, so $\boldsymbol{m_j^f}$ is the prior model parameter of the ensemble member *j*, and $\boldsymbol{m_j^a}$ is the model parameter of the ensemble member *j*, estimated at the updated state. $\boldsymbol{C_{MD}^f}$ is the cross-covariance matrix between the prior vector of model parameters $\boldsymbol{m^f}$, see Eq. (12), and the vector of predicted data, $\boldsymbol{d^f}$; $\boldsymbol{C_{DD}^f}$ (see Eq. (13)) is the auto-covariance matrix of the predicted data; $\boldsymbol{R}$ is the covariance matrix of the measurement errors, which can usually be assumed Gaussian. $\boldsymbol{d_{uc}}$ is the perturbed measurement data, $\boldsymbol{d_{uc}} \sim \boldsymbol{N}(\boldsymbol{d_{obs}}, \boldsymbol{R})$, with $\boldsymbol{d_{obs}}$ denoting the vector of the observed data.

$$\boldsymbol{C_{MD}^f} = \frac{1}{Ne-1}\left(\boldsymbol{m^f} - \frac{1}{Ne}\sum_{j=1}^{Ne}\boldsymbol{m_j^f}\right)\left(\boldsymbol{d^f} - \frac{1}{Ne}\sum_{j=1}^{Ne}\boldsymbol{d_j^f}\right)^T \tag{12}$$

$$\boldsymbol{C_{DD}^f} = \frac{1}{Ne-1}\left(\boldsymbol{d^f} - \frac{1}{Ne}\sum_{j=1}^{Ne}\boldsymbol{d_j^f}\right)\left(\boldsymbol{d^f} - \frac{1}{Ne}\sum_{j=1}^{Ne}\boldsymbol{d_j^f}\right)^T \tag{13}$$

ES assimilates the entire time series data and updates the model in one go, for nonlinear problems which may lead over correction and to get unacceptable results, so ES is not a popular method in reservoir history matching.

2.3 Ensemble smoother with multiple data assimilation (ESMDA)

Emerick et al. [Emerick and Reynolds (2012b)] published a multiple data assimilation (MDA) method, they assimilated the same data for multiple times, and they showed that MDA is superior to the single data assimilation in reservoir history matching. The ESMDA algorithm follows [Emerick and Reynolds (2012b)]:

Step 1: Arbitrarily select a number of data assimilations, *Na*, and the coefficients α_i for *i*= 1,…, *Na*, satisfying the following relationship:

$$\sum_{i=1}^{Na} \frac{1}{\alpha_i} = 1 \tag{14}$$

Step 2: The updating loops, for *i*=1 to *Na*:

a) Run the entire ensemble from the beginning (*t*=0).

b) For each realization of that ensemble, add white noise to the observation data using $\boldsymbol{d_{uc}} = \boldsymbol{d_{obs}} + \sqrt{\boldsymbol{\alpha_i}}\boldsymbol{R^{1/2}}\boldsymbol{z_d}$, where $\boldsymbol{z_d} \sim \boldsymbol{N}(\boldsymbol{0}, \boldsymbol{I})$.

c) Update the ensemble using the standard ES update equation

$$\boldsymbol{m_j^a} = \boldsymbol{m_j^f} + \boldsymbol{C_{MD}^f}(\boldsymbol{C_{DD}^f} + \boldsymbol{\alpha_i R})^{-1}(\boldsymbol{d_{uc,j}} - \boldsymbol{d_j^f}) \tag{15}$$

The ESMDA algorithm flow chart shows as Fig. 1**.**

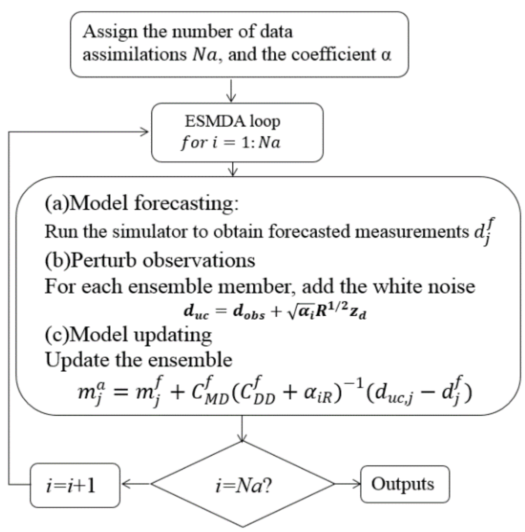

Figure 1: The algorithm flow chart of ESMDA

2.4 The derivation and application conditions of ESMDA

Inspired by Rommelse [Rommelse (2009)], Emerick et al. showed that in the linear Gaussian case, a MDA updates loop is equivalent to a single update, and the multiple data assimilation can improve the performance of the EnKF [Emerick and Reynolds (2012a)].

They extended the same idea into ES [Emerick and Reynolds (2012b)]. Here we review the fundamental of the derivation.

For linear problem as

$$\boldsymbol{d} = \boldsymbol{Gm} \tag{16}$$

If the probability of $\boldsymbol{m}$ has a Gaussian distribution. The prior model parameters $\boldsymbol{m^f} \sim N(\boldsymbol{m_{pr}}, \boldsymbol{C_M})$, therefore,

$$\boldsymbol{m^f} = \boldsymbol{m_{pr}} + \boldsymbol{C_M^{1/2} z_m} \tag{17}$$

where $\boldsymbol{z_m} \sim \boldsymbol{N}(\boldsymbol{0}, \boldsymbol{I})$.

We add the white noise to the measurement data to get $\boldsymbol{d_{uc}}$

$$\boldsymbol{d_{uc}} = \begin{bmatrix} \boldsymbol{d_{uc}^1} \\ \vdots \\ \boldsymbol{d_{uc}^{Na}} \end{bmatrix} \tag{18}$$

and $\boldsymbol{d_{uc}^i} \sim N(\boldsymbol{d_{obs}}, \boldsymbol{\alpha_i R})$, the superscript *i* indicate the *i*th data assimilation. The objective function of history matching is

$$\begin{aligned}\boldsymbol{O}(\boldsymbol{m}) = &\frac{\boldsymbol{1}}{\boldsymbol{2}}(\boldsymbol{m} - \boldsymbol{m^f})^{\boldsymbol{T}} \boldsymbol{C_M^{-1}} (\boldsymbol{m} - \boldsymbol{m^f}) \\ &+ \frac{\boldsymbol{1}}{\boldsymbol{2}} (\boldsymbol{Gm} - \boldsymbol{d_{uc}})^{\boldsymbol{T}} \boldsymbol{C_D^{-1}} (\boldsymbol{Gm} - \boldsymbol{d_{uc}})\end{aligned} \tag{19}$$

To minimize the objective function, the necessary condition is that the zero gradient of $\boldsymbol{O}(\boldsymbol{m})$, and its solution is

$$\widetilde{\boldsymbol{m}}^{\boldsymbol{a}} = \boldsymbol{C_{MAP}} \left\{ \boldsymbol{C_M^{-1}} \left(\boldsymbol{m_{pr}} + \boldsymbol{C_M^{\frac{1}{2}} z_m} \right) + \widetilde{\boldsymbol{G}}^{\boldsymbol{T}} \widetilde{\boldsymbol{C_D}}^{-\boldsymbol{1}} \left(\widetilde{\boldsymbol{d}}_{\boldsymbol{obs}} + \boldsymbol{C_D^{\frac{1}{2}}} \right) \right\} \tag{20}$$

where $\boldsymbol{C_{MAP}}$ is the covariance of the posteriori [Tarantola (2005)] , which can be expressed as

$$\boldsymbol{C_{MAP}} = \left(\boldsymbol{C_M^{-1}} + \boldsymbol{G^T C_D^{-1} G} \right)^{-\boldsymbol{1}} = \boldsymbol{C_M} - \boldsymbol{C_M G^T} \left(\boldsymbol{C_D} + \boldsymbol{G C_M G^T} \right)^{-\boldsymbol{1}} \boldsymbol{G C_M} \tag{21}$$

Define $\boldsymbol{m_{MAP}}$ is the maximum a posteriori, according to [Tarantola (2005)], it can be expressed as

$$\begin{aligned}\boldsymbol{m_{MAP}} &= \boldsymbol{C_{MAP}} \left(\boldsymbol{C_M^{-1} m_{pr}} + \boldsymbol{G^T C_D^{-1} d_{obs}} \right)^{-\boldsymbol{1}} \\ &= +\boldsymbol{C_M G^T} \left(\boldsymbol{C_D} + \boldsymbol{G C_M G^T} \right)^{-\boldsymbol{1}} (\boldsymbol{d_{obs}} - \boldsymbol{G m_{pr}})\end{aligned} \tag{22}$$

Because $m_{pr} \sim N(\boldsymbol{m_{MAP}}, C_{MAP})$, due to its Gaussianity, we only have to prove the following equations

$$\boldsymbol{E}[\widetilde{\boldsymbol{m}}^{\boldsymbol{a}}] = \boldsymbol{m_{MAP}} \tag{23}$$

$$\boldsymbol{COV}[\widetilde{\boldsymbol{m}}^{\boldsymbol{a}}] = \boldsymbol{E}[(\widetilde{\boldsymbol{m}}^{\boldsymbol{a}} - \boldsymbol{m_{MAP}})(\widetilde{\boldsymbol{m}}^{\boldsymbol{a}} - \boldsymbol{m_{MAP}})^{\boldsymbol{T}}] = \boldsymbol{C_{MAP}} \tag{24}$$

Based on Eq. (20), we write in the form of its expectation

$$\begin{aligned}
&\boldsymbol{E}[\widetilde{\boldsymbol{m}}^{\boldsymbol{a}}] = \boldsymbol{C_{MAP}}\left\{\boldsymbol{C_M^{-1}}\left(\boldsymbol{m_{pr}} + \boldsymbol{C_M^{\frac{1}{2}}}\boldsymbol{E}[\boldsymbol{z_m}] + \boldsymbol{G^T}\boldsymbol{C_D^{-1}}(\,\boldsymbol{d_{obs}} + \widetilde{\boldsymbol{C}}_{\boldsymbol{D}}^{\frac{1}{2}}\,\boldsymbol{E}[\widetilde{\boldsymbol{z_d}}]\right)\right\}\\
&=\boldsymbol{C_{MAP}}\{\boldsymbol{C_M^{-1}}\boldsymbol{m_{pr}} + \boldsymbol{G^T}\boldsymbol{C_D^{-1}}\,\boldsymbol{d_{obs}}\}\\
&=\boldsymbol{C_{MAP}}\left\{\boldsymbol{C_M^{-1}}\boldsymbol{m_{pr+}}[\boldsymbol{G^T}\dots\boldsymbol{G^T}]\begin{bmatrix}\frac{1}{\alpha_1}\boldsymbol{C_D^{-1}} & \cdots & \boldsymbol{0}\\ \vdots & \ddots & \vdots\\ \boldsymbol{0} & \cdots & \frac{1}{\alpha_{Na}}\boldsymbol{C_D^{-1}}\end{bmatrix}\begin{bmatrix}\boldsymbol{d_{obs}}\\ \vdots\\ \boldsymbol{d_{obs}}\end{bmatrix}\right\}\\
&=\boldsymbol{C_{MAP}}\left\{\boldsymbol{C_M^{-1}}\boldsymbol{m_{pr+}}[\boldsymbol{G^T}\dots\boldsymbol{G^T}]\begin{bmatrix}\frac{1}{\alpha_1}\boldsymbol{C_D^{-1}}\boldsymbol{d_{obs}}\\ \vdots\\ \frac{1}{\alpha_{Na}}\boldsymbol{C_D^{-1}}\boldsymbol{d_{obs}}\end{bmatrix}\right\}\\
&=\boldsymbol{C_{MAP}}\left\{\boldsymbol{C_M^{-1}}\boldsymbol{m_{pr}} + \left(\sum_1^{Na}\frac{1}{\alpha_i}\right)\boldsymbol{G^T}\boldsymbol{C_D^{-1}}\,\boldsymbol{d_{obs}}\right\}
\end{aligned} \tag{25}$$

The sufficient and necessary condition for Eq. (20) equals to Eq. (25) is

$$\left(\sum_1^{Na}\frac{1}{\alpha_i}\right)=1 \tag{26}$$

Similarly, we can prove

$$\begin{aligned}
&\boldsymbol{COV}[\widetilde{\boldsymbol{m}}^{\boldsymbol{a}}] = \boldsymbol{C_{MAP}}\left(\boldsymbol{C_M^{-1}} + \boldsymbol{G}\boldsymbol{C_M}\boldsymbol{G^T}\right)^{-1}\boldsymbol{C_{MAP}}\\
&= \boldsymbol{C_{MAP}}\left\{\boldsymbol{C_M^{-1}} + [\boldsymbol{G^T}\dots\boldsymbol{G^T}]\begin{bmatrix}\frac{1}{\boldsymbol{\alpha_1}}\boldsymbol{C_D^{-1}} & \cdots & \boldsymbol{0}\\ \vdots & \ddots & \vdots\\ \boldsymbol{0} & \cdots & \frac{1}{\boldsymbol{\alpha_{Na}}}\boldsymbol{C_D^{-1}}\end{bmatrix}\begin{bmatrix}\boldsymbol{G}\\ \vdots\\ \boldsymbol{G}\end{bmatrix}\right\}\boldsymbol{C_{MAP}}\\
&= \boldsymbol{C_{MAP}}\left\{\boldsymbol{C_M^{-1}} + \left(\sum_{1}^{Na}\frac{1}{\boldsymbol{\alpha_i}}\right)\boldsymbol{G^T}\boldsymbol{C_D^{-1}}\boldsymbol{G}\right\}\boldsymbol{C_{MAP}}\\
&= \boldsymbol{C_{MAP}}\{\boldsymbol{C_{MAP}^{-1}}\}\boldsymbol{C_{MAP}} = \boldsymbol{C_{MAP}}
\end{aligned} \tag{27}$$

The derivation is based on the assumption that $\boldsymbol{C_M}$ is a full rank matrix, which means an infinitely large ensemble size for ES (or EnKF). There are unlimited options of the coefficient α_i and *Na* satisfy Eq. (26), for linear problems with Gaussian distributions, they all give the correct posteriori. So, we summarize 3 conditions to apply ESMDA: 1) linear or near linear problems; 2) Gaussian distribution of the priori; 3) sufficiently large ensemble size.

The reservoir fluid simulator is a very complicated nonlinear function, but the relationships of oil rate, water cut, reservoir pressure to the permeability and porosity, within a certain range, can be regarded as a close linear function. For reservoir history matching problems, by balancing the efficiency and accuracy, the ensemble size should be larger than 100.

In comparison of EnKF and ESMDA, theoretically ESMDA has the advantage of significantly lower computational cost and shorter running time, due to the following two differences:

(1) EnKF is a recursive estimation which sequentially assimilate the measurement data once a step (usually one day as to match the daily production data), therefore the longer the production history, and the more assimilations will be made, and more accurate will the reservoir model be updated; whereas ESMDA is a smothering estimate which assimilate the entire history of the measurement dataset in one go, the user arbitrarily set a number of assimilating the same data multiple times, which number is usually quite small, resulting a much faster running time than EnKF.

(2) EnKF needs to store the state variables as Eq. (1) shows, and at each data assimilation step, EnKF uses the stored variables from the previous time step as the input to the simulator, to run only one step simulation. At the end of the entire data assimilation steps, it run the full simulation from day 0 to the end to check the consistency. This method not only take a large memory of the computer, but also potentially resulting severe inconsistency of the full-step and step-wise simulations; however, ESMDA does not restore those intermediate variables, because only a full-step simulation is required.

2.5 Geophysical and production data history matching workflow

Here we propose a standard workflow for geophysical and production data history matching.

Step 1: Initial ensemble Building. With the best geological knowledge through stochastic modeling to build the initial reservoir models.

Step 2: Production data preparation. Analyze the available well measurements, with certain quality control, eliminate the abnormal data with obvious errors.

Step 3: Geophysical data up-scaling. Usually seismic data has much finer grids than the reservoir modeling on the simulator, resulting a tremendous huge data to be much. To reduce the data size and computational cost, upscale or under sample a small but representative subset of the seismic data.

Step 4: Observation data rescaling. Geophysical data combined with production data forms the observation data to be history matched. Different kinds of measurement data and geophysical data may greatly varied with their magnitudes. Set proper rescaling factors for all the observation data have a similar magnitude.

Step 5: Set ESMDA history matching program (See **Chapter 2.3**), input the initial ensemble and rescaled observation data into the program.

Step 6: Check the validity of the updated ensemble. Inspect the updated reservoir models whether they are consistent with the geological understandings, run the reservoir simulator to see if the forecasted data matched the observation.

3 Case studies

Following the work flow we proposed, we conducted two case studies to test our ESMDA program. For both cases, we simulate a waterflood process on a synthetic reservoir. The reservoir structure model is from the SAIGUP project [Walsh and Manzocchi (2002)], which is 3D corner-point geometry, consists 40×120×20 cells, 78,720 of which are active cells. The permeability and porosity field is generated by sequential Gaussian simulation (SGSim), see Tab. 1. Both the porosity and the logarithm of permeability has a Gaussian distribution. The reservoir is assumed without any active aquifer, and the initial state is detailed in Tab. 2, and the relative permeability curve is shown in Fig. 2.

Table 1: Key parameters of the snythetic reference reservoir model

Parameters (Unit)	***Mean value***	***Variation***
Horizontal permeability (mD)	317.902	2.7519×10^{8}
Vertical permeability (mD)	31.7902	2.7519×10^{6}
Porosity	0.1160	0.29

Table 2: Initial state of the reservoir

Parameters	***Value (Unit)***
Initial reservoir pressure	300 (Bars)
Initial oil saturation	0.8
Initial water saturation	0.2

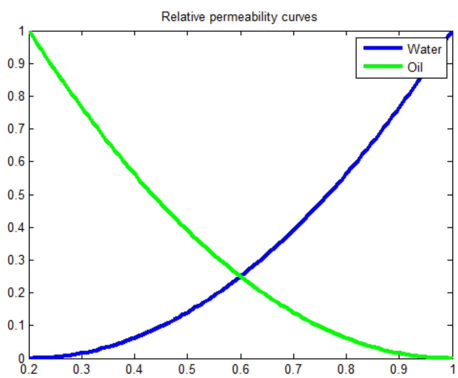

Figure 2: Relative permeability curve

The true reservoir is one realization of the SGSim, as the reference model, the other realizations are the initial reservoir models, see Fig. 3. The values of the permeability in the figures are shown in the unit of square meters. There are five injection wells and 5 producing wells. P1, P2,…, P5 are the oil producing wells, I1, I2,…, I5 are the water injection wells. All producing wells are operated under a constant bottomhole pressure (BHP) of 290 bars, and the injection wells are operated at a fixed injection rate of 500 m^3/d of water. We simulate the operation under that condition for 6570 days.

We build our own black-oil simulator with Implicit Pressure Explicit Saturation (IMPES) method on Matlab, with functions from Matlab reservoir simulation toolbox [Lie, Krogstad, Ligaarden et al. (2012)]. The input to the simulator includes the block-wise geological parameters and reservoir dynamic state variables, e.g., 3-way permeability and porosity, NTG, reservoir pressure and saturation, as well as the well operational parameters such as well location, BHP and water injection rates. The output of the simulator is the production data for this case study are well measurements, including well oil production rate, well water production rate and BHP. 4D seismic data we matched is primary wave (P-wave) impedance. Apply the ESMDA algorithm as we discussed above, and we set *Na*=4, α_1=α_2=α_3=α_4=4.

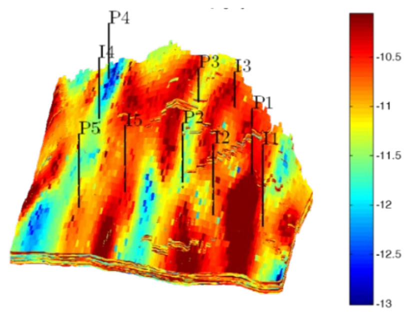

(a)

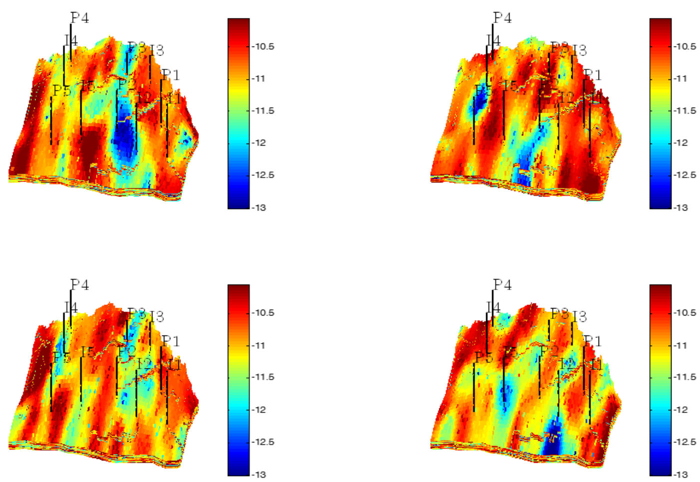

(b)

Figure 3: The water flooding operation well allocations and the horizontal permeability models of the reservoir: (a) reference model, and (b) 4 realizations of the prior models

By definition the P-wave impedance is shown in Eq. (28)

$$\boldsymbol{Z = \rho_{sat} V} \tag{28}$$

where z is the P-wave impedance, $\boldsymbol{\rho_{sat}}$ is the bulk density of the fluid saturated rock, and *V* is the acoustic velocity of the primary wave read from the log.

To model the density of saturated rocks, we used a linear average, also known as Wood's law, see Eq. (29)

$$\boldsymbol{\rho_{sat} = \emptyset \rho_f + (1 - \emptyset)\rho_m} \tag{29}$$

where ρ_f and ρ_m are the density of the saturating fluid and the density of the material constituting the rock matrix respectively, $\emptyset$ is porosity of the rock.

The P-wave velocity V can be calculated by applying Raymer's equation [Raymer, Hunt and Gardner (1980)], on the condition that porosity is smaller than 0.37, see Eq. (30).

$$\boldsymbol{V} = (\mathbf{1} - \emptyset)^2 \boldsymbol{V_{ma}} + \emptyset \boldsymbol{V_f} \tag{30}$$

where V_{ma} and V_f are the P-wave velocity of the material constituting rock matrix and the interstitial fluid respectively.

In the first case study, we only assimilate production data, the ESMDA updated models are shown in Fig. 4.

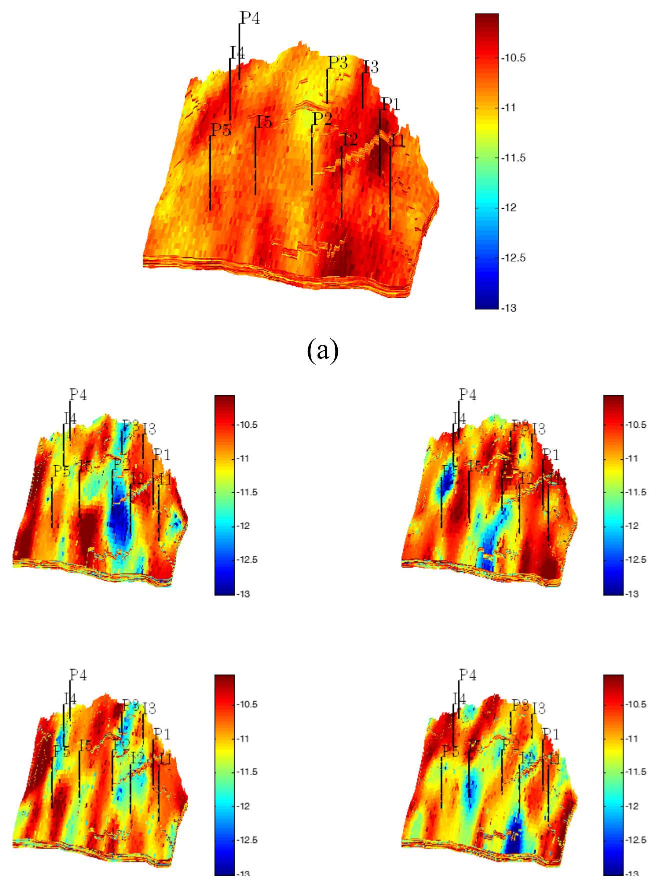

(a)

(b)

Figure 4: The ESMDA updated permeability models of the reservoir, assimilates production data only: (a) mean of all the 100 updated models, and (b) 4 realizations of the updated models

The production data we matched are the oil production rates and water production rates of the 5 producing wells, and the bottom-hole pressure (BHP) of the 5 water injection wells. Fig. 5 shows the production data matching result. The green solid lines are the forecasts from the prior models, the red dash line is the observed production data, and the black solid lines are the forecasts form the updated model applied the ESMDA algorithm on the production data only.

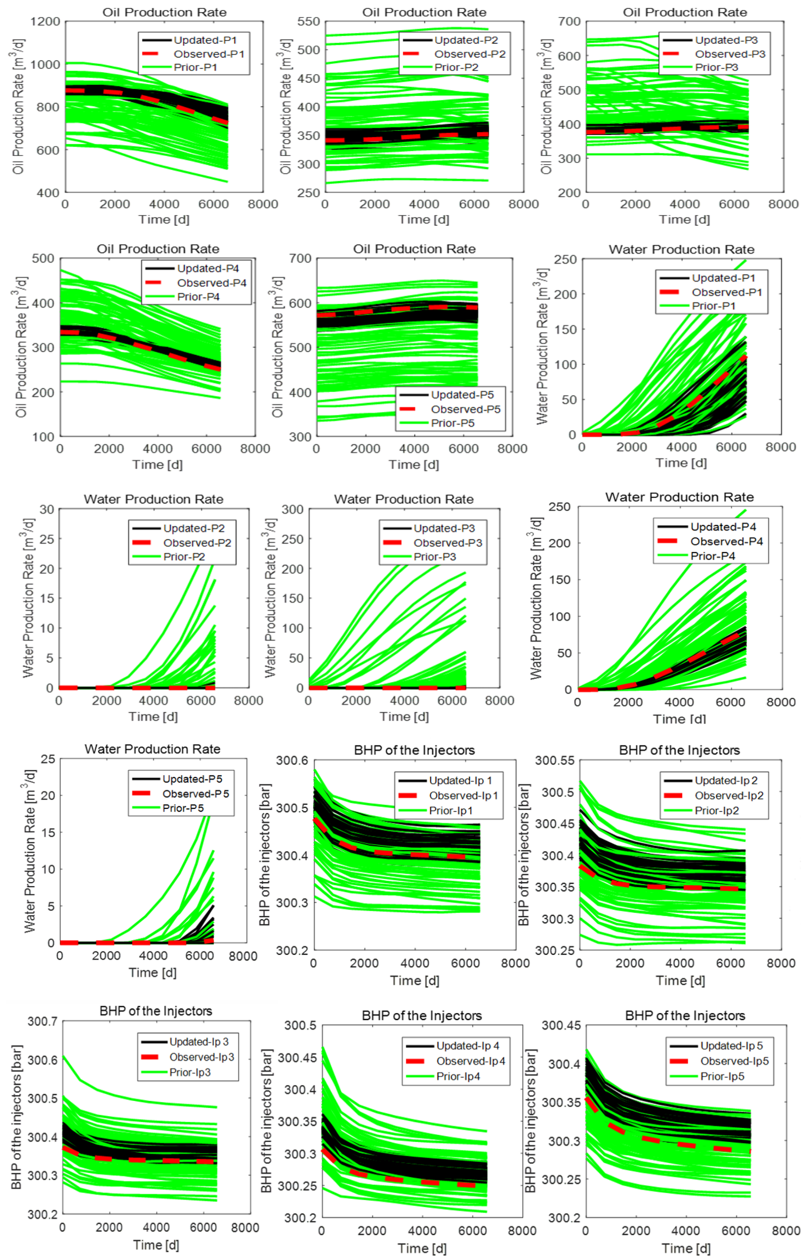

Figure 5: The results of history matching on the production data only

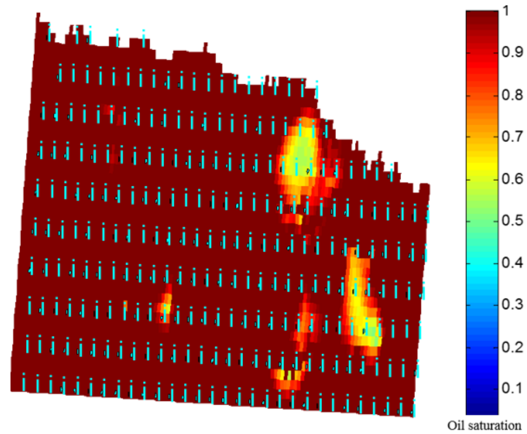

Figure 6: The top view of the P-wave impedance sampling points

In the second case study, besides the same production data assimilated in the first case study, we also integrated the 4D seismic data. In a waterflood operation, one important part is to locate the remaining oil, thus monitoring the fluid saturation change over time and space. P-wave impedance data directly reflect the saturation and porosity changes. In this case study, the pressure sensitivity can be neglected, so the porosity stays the same over years. Due to the extreme size of the P-wave impedance data set, we subsampled one P-wave impedance point in every 100 blocks, Fig. 6 shows the P-wave impedance spatial sampling points on the reservoir.

We assimilate the subsampled P-wave impedance for 10 times, in contrast, the well measurements are assimilated for 6570 times. Fig. 7 shows the ESMDA updated reservoir models.

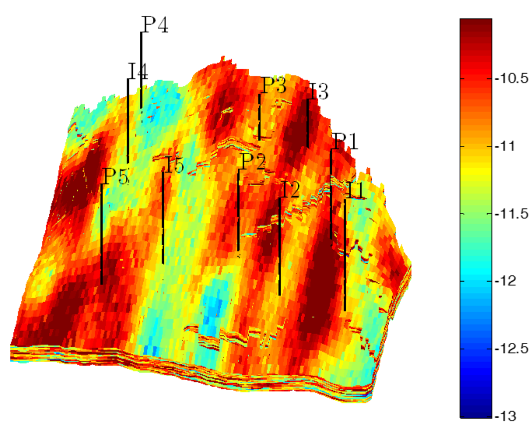

(a)

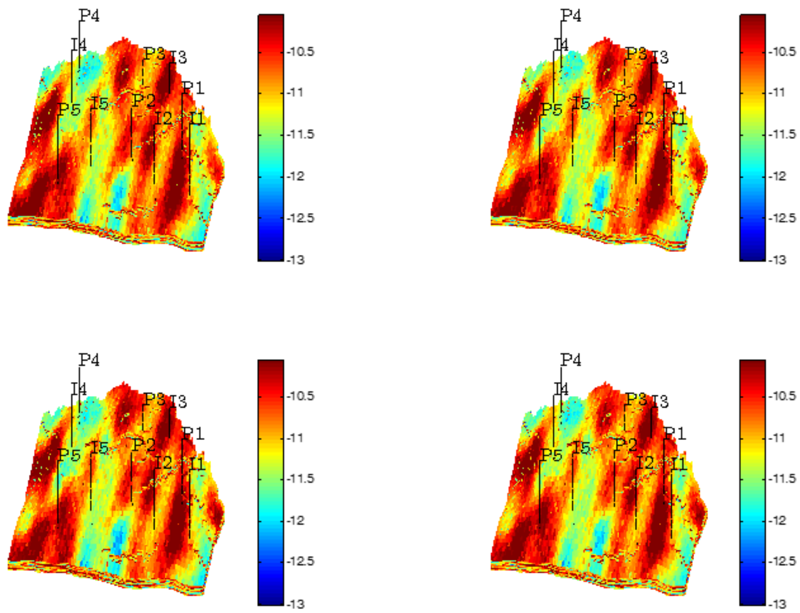

(b)

Figure 7: The ESMDA updated permeability models of the reservoir, assimilates production data and 4D seismic data: (a) mean of all the 100 updated models, and (b) 4 realizations of the updated models

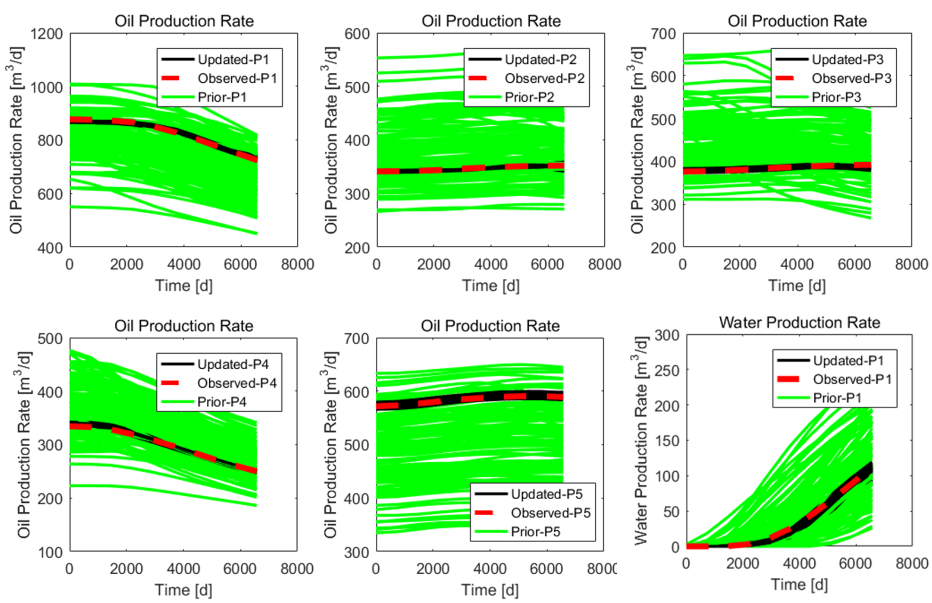

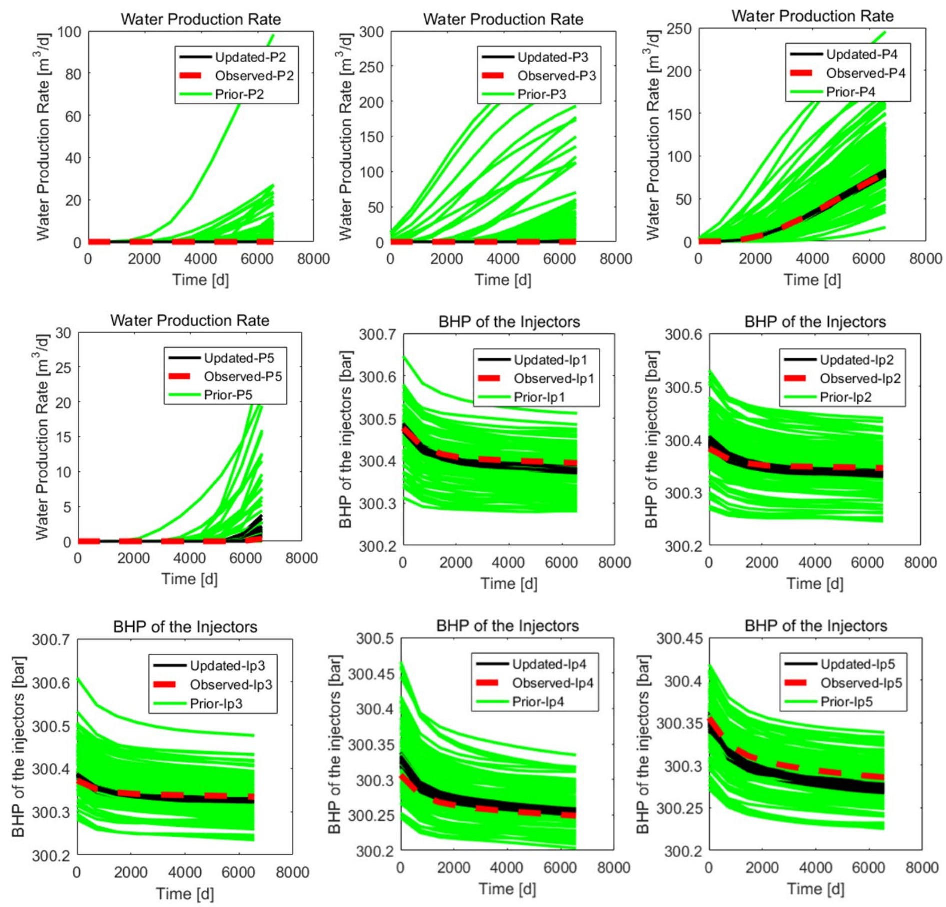

Figure 8: The results of history matching on both the production and the geophysical data

In order to quantitatively compare the accuracy of the forecasts from the update models of those two case studies, we defined the 2 sets of key statistical parameters of those forecasted data:

a) The percentage error of the mean of the updated model forecasts, which means the percentage of the absolute value of the difference between the mean of updated model predictions and its corresponding recorded data, over the same recorded data. We denote it as $\boldsymbol{e}$, see Eq. (31).

$$\boldsymbol{e} = \frac{\boldsymbol{abs}\left|\frac{\sum_{j=1}^{N} \boldsymbol{g}\left(\widehat{\boldsymbol{m}}^{\boldsymbol{u}}{}_{\boldsymbol{j}}\right)}{\boldsymbol{N}} - \boldsymbol{d_{obs}}\right|}{\boldsymbol{d_{obs}}} \times \mathbf{100}\% \tag{31}$$

To be more specific, on time t, the percentage errors on the oil rate, water production rate of the producing wells, denoted as $e_{oPi,t}$ and $e_{wPi,t}$; the percentage errors of the updated model forecasts on the BHP of the injection wells are denoted as $e_{bhpIi,t}$;

b) The variation of the updated forecasts, denoted as $\sigma^2{}_f$, see Eq. (32).

$$\sigma^2{}_f = \frac{\sum_{j=1}^{N}\left[g(\hat{m}^u{}_j) - \frac{\sum_{j=1}^{N} g(\hat{m}^u{}_j)}{N}\right]^2}{N} \tag{32}$$

To be more specific, on time t, $\sigma^2 o_{pi,t}$, $\sigma^2 w_{pi,t}$ and $\sigma^2 bhp_{Ii,t}$, which represents the variance of the updated forecasts on oil rate, water rate and BHP of the perspective wells, respectively.

For both sets of the statistical parameters, the subscript i=1, 2, 3, …, 5, indicating the well name numbers, the subscript t indicating the forecast on time t, and the subscript P and I indicating a producing well and an injection well respectively. Tabs. 3 and 4 shows those statistical parameters on day 6570, which is the last day of the history matching. The percentage errors and the variance from Case study 2 is generally much smaller than those from Case study 1, indicating a higher confidence in the forecasts from the updated models in Case study 2.

Table 3: Percentage errors of case study 1 and case study 2, on day 6570

	$e_{oP1,6570}$	$e_{oP26570}$	$e_{oP3,6570}$	$e_{oP4,6570}$	$e_{oP5,6570}$
Case study 1	4.1%	1.84%	0. 7%	2.7%	1.9%
Case study 2	2.6%	1.6%	1.6%	1.1%	1.9%
	$e_{wP1,6570}$	$e_{wP26570}$	$e_{wP3,6570}$	$e_{wP4,6570}$	$e_{wP5,6570}$
Case study 1	23%	0%	170%	11.8%	13.6%
Case study 2	3.3%	0%	16%	6.8%	35%
	$e_{bhpI1,657}$	$e_{bhpI2657}$	$e_{bhpI3,6570}$	$e_{bhpI4,657}$	$e_{bhpI5,6570}$
Case study 1	0.006%	0.007%	0.006%	0.006%	0.008%
Case study 2	0.007%	0.006%	0.009%	0.003%	0.005%

Table 4: Variances of case study 1 and case study 2, on day 6570

	$\sigma^2 o_{P1,6570}$	$\sigma^2 o_{P2,6570}$	$\sigma^2 o_{P3,6570}$	$\sigma^2 o_{P4,6570}$	$\sigma^2 o_{P5,6570}$
Case study 1	503.15	33.39	69.78	18.9	83.53
Case study 2	10.13	3.12	2.68	1.49	4.42
	$\sigma^2 w_{P1,6570}$	$\sigma^2 w_{P2,6570}$	$\sigma^2 w_{P3,6570}$	$\sigma^2 w_{P4,6570}$	$\sigma^2 w_{P5,6570}$
Case study 1	514.80	0.012	2.61	31.54	1.28
Case study 2	6.44	0.10	0.11	2.36	0.05
	$\sigma^2 bhp_{I1,657}$	$\sigma^2 bhp_{I2,6570}$	$\sigma^2 bhp_{I3,657}$	$\sigma^2 bhp_{I4,657}$	$\sigma^2 bhp_{I5,657}$
Case study 1	2.94 st^{-4}	1.82 s0^{-4}	1.42 s0^{-4}	6.31 s0^{-5}	9.52 s0^{-5}
Case study 2	4.49 st^{-6}	7.09 st^{-6}	7.25 st^{-6}	3.00 st^{-6}	2.44 st^{-6}

By visually comparing the Figs. 5 and 8, it is also clearly the integration of the seismic and production data ESMDA history matching yields a superior results both in model updating and the well measurements matching. And from Figs. 7 and 4, with the assimilation on 4D seismic data in case study 2, each updated reservoir realizations captured the correct high permeability pathways, resulting the mean of those realizations are more resemble to the “true” reservoir: however, in case study, the each updated reservoir realizations varied in their permeability patterns, resulting the mean of those realizations less informative in showing the real geological features.

We also recorded the CPU running time for these two case studies. The program has been run on a workstation HP® Z240, with dual 3.50 GHz Intel® Xeon® CPU E3-1240 v5. The entire elapsed time for case study 1 is 11276.176 seconds; for the second case study, even though with the additional subsampled geophysical data, the observation vector d_{uc} almost doubled its size, the entire elapsed time is almost the same, resulting as 11287.026 seconds. These two case studies share the same number of simulation runs (500 runs each). This shows the CPU running time is not noticeable influenced by the vector size, due to effective high matrix computing functions from Matlab.

Seismic data not only provide the structural constraints on geology, some seismic attributes (e.g., P-wave impedance) also reflects the fluids change in reservoir. With the additional information from the seismic data, the model corrections are more significant and accurate. Moreover, after a well interpreted seismic data and with a carefully designed subsampling method, integrating geophysical data into history matching does not require much additional computing cost.

4 Conclusions

In this paper, we reviewed the EnKF and ES inverse modeling methods and their formulations, and we derived the ESMDA, discussed its application scope, and compared the two cases studies on the ESMDA reservoir inverse modeling, one with only production data assimilation, the other integrate the seismic data and production data together. The following conclusions are obtained:

a) For linear problems, ES is equivalent to Gauss-Newton, and it can assimilate the entire time series data and update the model in on go. ES has the highest efficiency among the ensemble based methods we discussed.

b) For nonlinear problems, e.g., reservoir fluid simulator, ES gives unacceptable results, due to its overcorrection. ESMDA was proposed for reservoir inverse modeling problems.

c) ESMDA is superior to the EnKF in assimilation time scarce seismic data, and higher computing efficiency in time dense data assimilation.

d) 4D seismic provide an additional information with fluid changes in reservoir to estimate the spatial reservoir properties. The integration of seismic and production history matching yields a superior result.

Acknowledgement: This work is financially supported by Chinese National Science and Technology Major Project (2016ZX05015-005). The first author also gratefully acknowledged the University of Wyoming for facilitating the research, as well as Dr. Dario Grana and Dr. Aryana’s professional guidance.

Conflicts of Interest: The authors declare that they have no conflicts of interest to report regarding the present study.

References

Aanonsen, S.; Nævdal, G.; Oliver, D.; Reynolds, A.; Vallès, B. (2009): The ensemble Kalman filter in reservoir engineering—a review. *SPE Journal*, vol. 14, pp. 393-412.

Bhakta, T.; Luo, X.; Nævdal, G. (2016): Ensemble based 4D seismic history matching using a sparse representation of AVA data. *SEG International Exposition and 86th Annual Meeting, Dallas, Texas, USA.*

Chen, Y.; Oliver, D. (2013): Levenberg-Marquardt forms of the iterative ensemble smoother for efficient history matching and uncertainty quantification. *Computational Geosciences*, vol. 17, no. 4, pp. 689-703.

Emerick, A. A.; Reynolds, A. C. (2012a): Ensemble smoother with multiple data assimilation. *Computers & Geosciences*, vol. 55, pp. 3-15.

Emerick, A. A.; Reynolds, A. C. (2012b): History matching time-lapse seismic data using the ensemble Kalman filter with multiple data assimilations. *Computational Geosciences*, vol. 16, no. 3, pp. 639-659.

Emerick, A. A.; Reynolds, A. C. (2013): History-matching production and seismic data in a real field case using the ensemble smoother with multiple data assimilation. *SPE Reservoir Simulation Symposium, Society of Petroleum Engineers.*

Evensen, G. (2009): *Data Assimilation the Ensemble Kalman Filter, 2nd Edition.* Springer.

Evensen, G.; Van Leeuwen, P. J. (2000): An ensemble Kalman smoother for nonlinear dynamics. *Monthly Weather Review*, vol. 128, no. 6, pp. 1852-1867.

Gao, G.; Li, G.; Reynolds, A. C. (2004): A stochastic optimization algorithm for automatic history matching. *SPE Annual Technical Conference and Exhibition, Houston, Texas, USA.*

Gu, Y.; Oliver, D. (2007): An iterative ensemble Kalman filter for multiphase fluid flow data assimilation. *SPE Journal*, vol. 12, pp. 438-446.

Helland, R.; Festervoll, K.; Stronen, L. K.; Youness, E. O. (2008): Successful IOR implementation at the Gullfaks field. *19th World Petroleum Congress, Spain 2008 Forum 2.*

Leeuwenburgh, O.; Arts, R. (2014): Distance parameterization for efficient seismic history matching with the ensemble Kalman Filter. *Computational Geosciences*, vol. 18, pp. 535-548.

Le, D. H.; Emerick, A. A.; Reynolds, A. C. (2015): An adaptive ensemble smoother with multiple data assimilation for assisted history matching. *SPE Reservoir Simulation Symposium, Houston, Texas, USA.*

Le, D. H.; Younis, R. A; Reynolds, A. C. (2015): A history matching procedure for non-Gaussian facies based on ES-MDA. *SPE Reservoir Simulation Symposium, Houston, Texas, USA.*

Li, G.; Reynolds, A. C. (2009): Iterative ensemble Kalman filters for data assimilation. *SPE Journal*, vol. 14, pp. 496-505.

Lie, K. A.; Krogstad, S.; Ligaarden, I. S.; Natvig, J. R.; Nilsen, H. M. et al. (2012): Open source MATLAB implementation of consistent discretisations on complex grids. *Computational Geosciences*, vol. 16, no. 2, pp. 297-322.

Lumley, D.; Adams, D.; Meadows, M.; Cole, S.; Ergas, R. (2003): 4D seismic pressure-saturation inversion at Gullfaks field, Norway. *First Break*, vol. 21, no. 9.

Luo, X.; Stordal, A.; Lorentzen, R.; Nævdal, G. (2015): Iterative ensemble smoother as an approximate solution to a regularized minimum-average-cost problem: theory and applications. *SPE Journal*, vol. 20, pp. 962-982.

Nævdal, G.; Johnsen, L. M.; Aanonsen, S. I.; Vefring, E. H. (2005): Reservoir monitoring and continuous model updating using ensemble Kalman filter. *SPE Journal*, vol. 10, pp. 66-74.

Nocedal, J.; Wright, S. (2000): *Numerical Optimization, 2nd Edition*. Springer.

Oliver, D. S.; Reynolds, A. C.; Liu, N. (2008): *Inverse Theory for Petroleum Reservoir Characterization and History Matching*. Cambridge University Press.

Raymer, L. L.; Hunt, E. R.; Gardner, J. S. (1980): An improved sonic transit time-to porosity transform. *SPWLA 21st Annual Logging Symposium, Lafayette, USA.*.

Reynolds, A. C.; Zafari, M.; Li, G. (2006): Iterative forms of the ensemble Kalman filter. *10th European Conference on the Mathematics of Oil Recovery, Amsterdam.*

Rommelse, J. (2009): *Data Assimilation in Reservoir Management (Ph.D. Thesis),* Technical University of Delft, Delft, The Netherlands.

Skjervheim, J.; Evensen, G. (2011): An ensemble smoother for assisted history matching. *SPE Reservoir Simulation Symposium, Woodlands, Texas, USA.*

Talukdar, S.; Instefjord, R. (2008): Reservoir management of the Gullfaks main field. *SPE Europec/EAGE Conference, Rome, Italy.*

Tarantola, A. (2005): *Inverse Problem Theory and Methods for Model Parameter Estimation*. SIAM, Philadelphia, USA.

Tolstukhin, E.; Lyngnes, B.; Sudan, H. H. (2012): Ekofisk 4D seismic history matching workflow. *EAGE Annual Conference & Exhibition Incorporating SPE Europec, Copenhagen, Denmark.*

Trani, M.; Arts, R.; Leeuwenburgh, O. (2012): Seismic history matching of fluid fronts using the ensemble Kalman filter. *SPE Journal*, vol. 18, no. 1, pp. 159-171.

Van Leeuwen, P. J.; Evensen, G. (1996): Data assimilation and inverse methods in terms of a probabilistic formulation. *Monthly Weather Review*, vol. 124, no. 12, pp. 2898-2913.

Wang, Y.; Sun, S. (2016): Direct calculation of permeability by high-accurate finite difference and numerical integration methods. *Communications in Computational Physics*, vol. 20, no. 2, pp. 405-440.

Wang, Y.; Sun, S.; Yu, B. (2017): Acceleration of gas flow simulations in dual-continuum porous media based on the mass-conservation POD method. *Energies*, vol. 10, no. 9, pp. 1380-1397.

Wang, Y.; Sun, S.; Gong, L.; Yu, B. (2018): A globally mass-conservative method for dual-continuum gas reservoir simulation. *Journal of Natural Gas Science and Engineering*, vol. 53, pp. 301-316.

Wang, Y. (2019): Reynolds stress model for viscoelastic drag-reducing flow induced by polymer solution. *Polymers*, vol. 11, no. 10, pp. 1659-1675.

Wang, Y.; Wang, Y.; Cheng, Z. (2019): Direct numerical simulation of gas-liquid drag-reducing cavity flow by the VOSET method. *Polymers*, vol. 11, no. 4, pp. 596-611.

Walsh, J. J.; Manzocchi, T. (2002): SAIGUP Project-Impact of geological uncertainties on production from clastic reservoirs. *64th EAGE Conference & Exhibition, Florence, Italy.*